Generalised Correlations of Blow-off and Flame Quenching for Sub-sonic and Choked Jet Flames

Adriana Palacios[1]*, Derek Bradley[2]

[1]Fundacion Universidad de las Americas, Puebla, Department of Chemical, Food and Environmental Engineering, Puebla 72810, Mexico.

[2]University of Leeds, School of Mechanical Engineering, Leeds LS2 9JT, UK.

*Corresponding author email: adriana.palacios@udlap.mx

ABSTRACT

Dimensionless groups suggested by the mathematical modelling of subsonic fuel jet flames, and extensive experimental data, have been reasonably successsful in correlating dimensionles flame heights and flame lift-off distances in terms of a dimensionless flow number. This approach is extended to the more exacting correlations that define regimes of flame quenching, blow-off, and lifted flames. Experimental data from these diverse sources are analysed, and the bounds of these regimes are expressed in terms of the critical minimum jet pipe diameter to avoid blow-off, normalised by the laminar flame thickness for the maximum burning velocity mixture, and the flow number. The regimes extend from low Reynolds number laminar flows in hypodermic tubes to high Reynolds number choked flows, with supersonic shocks.

Data are well corrrelated in the subsonic regime for a range of hydrocarbon gases, in which critical pipe diameters for the avoidance of blow-off increase with flow number. Matters are more complex in the extended choked flow regime, in which there are less data. This regime of supersonic flow and shock waves is one of improved fuel/air mixing and enhanced reactivity, to such an extent that the critical pipe diameter, after reaching a maximum, decreases. Data are presented in this regime, and indeed over the full range of conditions, for methane, propane and hydrogen jet flames. Hydrogen exhibits more reactive characteristics than the hydrocarbons. In terms of the correlating parameters, whereas laminar flame thickness is related to that of the non-reacting preheat zone, such a zone is difficult

to define with hydrogen, as a consequence of the upstream diffusion of H atoms, and this aspect is discusssed.

KEYWORDS: critical pipe diameter, choked flow, flame quench, lifted flames, hydrocarbons blow-off, hydrogen blow-off.

NOMENCLATURE

a	acoustic velocity (m/s)
C_p	specific heat at constant pressure (J/kg K)
D	pipe diameter (m)
D_b	critical pipe diameter, below which blow-off occurs (m)
f	ratio of fuel to air moles in fuel-air mixture for maximum laminar burning velocity, S_L
H	flame height (m)
k	thermal conductivity (W/m K)
L	flame lift-off distance (m)
M	Mach number
P_a	atmospheric pressure (Pa)
P_i	initial stagnation pressure (Pa)
S_L	maximum laminar burning velocity of the fuel-air mixture under conditions of ambient atmosphere (m/s)
t	time (s)
T	temperature (K)
T^o	temperature at inner layer of laminar flame (K)
u	fuel flow mean velocity at the exit plane of pipe for subsonic flow. For ratios of atmospheric pressure to P_i equal to, or less than the critical pressure ratio. Also choked sonic velocity after isentropic expansion from P_i (m/s)
U*	dimensionless flow number for choked and unchoked flow, $(u/S_L)(\delta/D)^{0.4}(P_i/P_a)$
U_b*	U* value at blow-off

Greek

δ	laminar flame thickness, for S_L under conditions of ambient atmosphere, (ν/S_L) (m)
δ_k	$(k/C_p)_{T^o}/\rho_u S_L$ (m), see Eq. (4)
ϕ	equivalence ratio
γ	ratio of specific heats
η	dynamic viscosity (kg/m s)
ν	kinematic viscosity, under conditions of ambient atmosphere (m^2/s)
ρ	density (kg/m^3)

Subscripts

a	ambient conditions
i	initial stagnation conditions
u	unburned gas

1. INTRODUCTION

As the velocity of a jet flame increases, so also does the flame lift-off distance. Eventually, the flow becomes unstable and oscillatory, leading to flame blow-off. Although there are valuable correlations of plume heights and flame lift-off distances in subsonic and supersonic flows, there is much less guidance about the onset of flame blow-off, in both subsonic and choked flows. The increasing use of "fracking", with its associated flaring, with possible incomplete combustion and emissions of a potent greenhouse gas, emphasises the importance of further studies in this area. Jet flames can also arise from

high pressure, small diameter, fuel leakages, while hydrogen venting from malfunctioning nuclear reactors presents a formidable challenge.

The present paper discusses data on blow-off, in the absence of cross winds, and addresses the problems of correlating these for some of the more common fuels, in both the subsonic and choked flow regimes. All the flames considered are located on a cylindrical pipe, discharging pure fuel vertically, in the absence of any pilot flame. The presence of cross winds [1] can reduce combustion efficiency, as can the presence of inert gas, such as nitrogen and carbon dioxide [2], as well as air [3,4]. A review of the extensive experimental data on jet flame heights and lift-off distances is presented in [5]. The associated detailed flame structure of lifted hydrocarbon turbulent jet flames and their stability has been discussed by Lyons [6], along with a review of turbulent lifted flame theories.

The analysis and mathematical modeling of lift-off distances, the associated flame structures, and blow-off in both flow regimes presents severe problems. This is due to the complexities of mixing at high turbulence, many different chemical reactions at high strain rates, flamelet curvatures, and localised flame extinctions that lead to blow-off. Instabilities are generated at both very low flow rates and also just prior to blow-off, creating a very severe modeling test [7].

Results from the subsonic stretched laminar flamelet modelling in [8], in conjunction with experimental jet flame data, have led to a practical correlation of the normalised flame heights, in terms of a dimensionless flow number, U*, given by [5]:

$$U^* = (u/S_L)(\delta/D)^{0.4}(P_i/P_a). \qquad (1)$$

Here, u is the pipe flow mean subsonic velocity or, in choked flow, the sonic velocity, D the pipe diameter, S_L the maximum burning velocity of the fuel/air mixture, under conditions of the ambient atmosphere at a pressure P_a, and δ the laminar flame thickness for S_L at the ambient conditions. The pressure ratio P_i/P_a is the initial stagnation pressure normalised by P_a. In the absence of (P_i/P_a), U* has affinities with the Karlovitz stretch factor, employed in the characterisation of premixed turbulent flames [9]. Increases in both of these two related parameters are associated, not only with increases in burn rate, but also with eventual flame quench, leading, in the case of jet flames, to blow-off at a critical value

of the pipe diameter, D_b, normalised by δ. An aim of the present study is the derivation of values of U*, at blow-off, namely U_b*, for a given fuel and the associated critical dimensionless pipe diameter, D_b/δ, below which blow-off occurs.

The complexities, referred to above, are severely aggravated with choked flow and the associated over-pressure at the pipe exit. This is because increases in P_i/P_a are followed by non-isentropic expansions, creating supersonic velocities, and shock wave transitions. The dimensionless groups, created in [5], as result of mathematical modelling [8,10], are employed, in conjunction with the extensive experimental data on blow-off, from a large number of sources in [5], to correlate blow-off conditions for both subsonic and choked flows. In choked flow the influences of the pressure ratio, P_i/P_a, and the shock structure become dominant, influencing both U_b* and D_b/δ.

Some fundamental aspects of flame lift-off distance, L, and the nature of choked flow are first considered. Data on blow-off in both subsonic and choked flows of methane, hydrogen, and propane are then scrutinised and correlated. The data also cover flame quenching at low Reynolds number laminar jet flows from hypodermic tubes. Blow-off data in the subsonic regime also are presented for acetylene, ethylene, and butane.

2. LIFT-OFF DISTANCE, SUBSONIC AND CHOKED BLOW-OFF

The mathematical modelling in [8] and [10] shows that the intense mixing that exists between the exit plane of the fuel jet and the flame leading edge, generates high strain rates. These decay downstream, but upstream they are high enough initially to inhibit combustion. The mathematical modelling shows how, after turbulent jet mixing, the most reactive flamelets, somewhat richer than stoichiometric, become established in a region that combines high reactivity with sufficiently high flame extinction stretch rates for flame survival. However, as U* increases, with the increasing air dilution, the flamelets become leaner, their thickness increases, whilst their flame extinction stretch rate decreases. As a consequence, localised flame extinctions increase and the flame eventually blows off [8,10]. The computations in [8] show that a smaller pipe diameter gives better penetration of the air and greater leaning-off of the mixture, leading to earlier localised flame extinctions and blow-off.

Details of how a blow-off develops were studied experimentally by AP at the State Key Laboratory in Fire Science, Hefei. Subsonic jet flames of methane and propane were employed, with pipe diameters ranging between 3 and 8 mm, as described in [4]. Fig. 1(a) shows the sharp increase in the normalised lift-off distance, (L/D)f, just prior to blow-off of a methane jet, as a function of U*. Here f is the ratio of fuel to air moles at the maximum value of S_L [5]. The pipe diameter was 3 mm and the velocity was varied between 19.5 and 32 m/s, with corresponding values of U* of 9 and 14.8.

Fig. 1(b) shows the fluctuations in lift-off distance that develop at a fixed point just prior to blow-off. The amplitude of the fluctuations increases sharply as blow-off is approached. The U* value for the methane jet flame was 10.3. The values of U_b* currently employed will be those of U* that just sustain a lifted flame prior to the development of such instabilities.

In [5] the lift-off distance relationship within the subsonic regime is given by:

$$(L/D)\,f = 0.11U^* - 0.2\,. \qquad (2)$$

The f ratio is important in the correlations, because different fuels have different air requirements.

When the ratio of the pressure at the pipe exit plane, P, to the initial stagnation pressure, P_i, decreases with increasing P_i and attains the critical pressure ratio, CPR, the jet velocity becomes equal to the acoustic velocity. The flow becomes choked, in that the sonic velocity is maintained with any further increase in P_i. The localised pressure of the fuel jet at the pipe exit plane is P_i, multiplied by the CPR. With increasing P_i the leaving pressure progressively increases above the atmospheric pressure. Further expansion of the high density jet could occur, near-isentropically, in a convergent-divergent nozzle, but this is seldom the practice with jet flames. The fluid mechanics relationships for isentropic changes in the jet flow relevant to the present study are summarised in the Appendix.

Changes in the flow pattern due to the increasing pressure in choked flow have been summarised by Ewan and Moodie in [11]. Figure 2 is taken from this paper, and shows the creation of expansion waves at the edge of the discharge pipe, and reflected at the outer boundary as compression waves. Their coalescence results in a barrel-shaped shock, surrounding a supersonic region that arises from the further expansion of the gas. This

culminates in a normal shock wave, or Mach disc, downstream of which, subsonic flow is surrounded by supersonic flow.

It was found that with P_i/P_a = 8, the barrel length was about 2.5D, and the Mach disc diameter was about 1.4D [11]. Subsonic jet flames become anchored downstream of the Mach disc [12]. Within this regime, there is a significant increase in the reaction rate. This can be attributed to several factors: the increasing mass flux of fuel due to the increasing fuel density, ensuing improved fuel/air mixing, large gradients of velocity and fuel concentration, together with the generation of the barrel shock and Mach disc. All of these are associated with an increase in P_i/P_a and the increasingly choked flow. The expansion wave and reflected shocks, have a profound effect in changing, and enhancing, downstream combustion.

These effects become dominant, influencing both U_b* and δ/D_b. Soon after the CPR has been attained, there is a regime of minimal reactivity, quickly followed by one in which it increases. The subsonic correlation, Eq. (2), is no longer valid and is superseded within the sonic and supersonic regime by [5]:

$$(L/D)\, f^{0.2} = -54 + 17\ln(U^* - 23). \qquad (3)$$

The lift-off distance relationships in both separated regimes are shown in Fig. 3, modified from a figure in [5]. The half-filled data points and the correlating upper curve is indicative of the sonic/supersonic regime and Eq. (3). The lower data points and curve correspond to the subsonic regime and Eq. (2).

3. CORRELATIONS OF FLAME BLOW-OFF

3.1 Values of δ/D_b

A number of workers have measured the conditions for blow-off over both the subsonic and choked flow regimes, principally for methane, hydrogen, and propane, in a variety of different ways. For example, Birch et al. [13,14] measured the pressure at which blow-off occurs with a particular pipe diameter, and plotted P_i/P_a against D_b, while Kalghatgi [15] plotted the Mach number at the pipe exit against D_b. Butler et al. [16] plotted mass flow

rate against pipe diameter in the flame quench regime. For many other fuels blow-off data have been confined to the subsonic regime.

The different measured parameters that have been employed are re-expressed in terms of the present dimensionless groups. The relevant jet flow equations to do this are numbered and given in the Appendix. Table 1 lists the different Appendix equation numbers that have been employed for the different types of experimental data. Values of the necessary physico-chemical properties at the value of ϕ for the maximum laminar burning velocity, for mixtures at 0.1MPa and at 50 kPa, at 300K are given with the source references in Table 2. Throughout the paper the necessary thermo-physical data were obtained from the Gaseq equilibrium code [26].

For a given fuel and pipe diameter, the correlations present the limiting conditions for blow-off, in terms of the flow number, U*. At this condition $U^* = U_b^*$ and D_b, is the smallest pipe diameter, that can still maintain a lifted flame. Blow-off occurs, when $D < D_b$ or, more generally, $\delta/D > \delta/D_b$.

The laminar flame thickness, δ, is approximated by the thickness of the preheat zone at the maximum laminar burning velocity, S_L, in its conveniently simple form, $\delta = \nu/S_L$. More accurately, this should be divided by the mixture Prandtl number, $= \eta C_p/k$. Even greater accuracy for this thickness is given by the expression derived by Göttgens et al. [27]. This involves the identification of an inner layer, the thickness of which is defined by the location of a temperature T^o, below which there is no reaction. Calculated values of T^o are presented in [27] for CH_4, H_2, C_3H_8, C_2H_2 and C_2H_4 mixtures with air. For hydrocarbon flames the chemically inert preheat zone thickness is approximately equal to the flame thickness and the thickness of this zone, defined here as δ_k, is evaluated from:

$$\delta_k = \frac{(k/C_p)_{To}}{\rho_u S_L}, \qquad (4)$$

where $\left(k/C_p\right)_{T^o}$ is evaluated at T^o. Values of ϕ for S_L, relevant to the present study, T^o, δ, and δ_k, predominantly at 0.1 MPa and 300K, but with additional C_3H_8 data at 50 kPa, are presented in Table 3.

Combined subsonic and choked data are now presented, in turn, for the blow-off characteristics of methane, hydrogen, and propane jet flames. The correlation curves take the form of plots of δ/D_b and P_i/P_a against U_b*. Data sources are given on the appropriate figures. Subsonic data are also presented for acetylene, butane and ethylene. The characteristic curves also show the regime of quenched flames, discussed in Section 4.1. Over a wide range of conditions the curves define regimes in which lifted flames are possible.

The onset of the choked regime occurs when P_i/P_a attains the value of the CPR, with P_a = 0.1 MPa. This is indicated on the plots of δ/D_b against U_b* by a dashed vertical line. Thereafter, with further increase in P_i/P_a, the pressure at the pipe exit plane increases, with u the choked fuel flow velocity. The associated value of U_b* increases, while δ/D_b decreases, and then increases as shocked flows develop.

3.2. Methane

Correlation curves for methane jet flames, drawn from a variety of sources, are shown in Fig. 4. These include values of these parameters derived from the measurements of Birch et al. [13], who studied blow-off stability limits in both the subsonic and choked flow regimes with high pressure natural gas jets. As in the work of McCaffrey and Evans [12], they measured the critical pipe diameters, D_b, below which, the flame became unstable, and blow-off occurred. For diameters greater than D_b, below the δ/D_b curve in Fig. 4 is the regime of stable lifted flames. Above it, at the smaller values of D_b, blow-off has occurred and a flame cannot be sustained. In the choked flow regime, u is equal to the acoustic speed. As P_i/P_a increases in the subsonic regime, so also does u, until the falling value of P_a/P_i attains the critical pressure ratio, of 0.544 at 0.1 MPa and 300 K, with P_i/P_a = 1.84. This limit is shown by the dashed vertical line. At the higher values of P_i/P_a and U_b* the

mean velocity at the pipe exit plane remains at the sonic velocity and flow patterns, of the type indicated in Fig. 2, develop. The experimental pipe diameters ranged between 5.5 and 38.1 mm.

Kalghatgi [15] measured blow-off conditions in the subsonic regime, with burner diameters ranging between 0.2 and 12 mm for hydrogen, methane, propane, ethylene, acetylene and commercial butanes. Values of blow-off Mach number at the burner exit were plotted against the burner diameter. Figure 4 shows these data for methane after re-processing and using the transformative equations listed in Table 1.

Annushkin and Sverdlov [17] also obtained blow-off data in both regimes. They directed jets into a pressure chamber, the ambient pressure of which could be varied. Their experimental data effectively show the minimal critical pipe diameters that might sustain a lifted flame, as a function of P_i/P_a -1. Here only the atmospheric ambient findings are considered. The necessary transformative equations are again also listed in Table 1. Data for the quench regime, described in Section 3.5, are drawn from the experimental data reviewed by Butler et al. [16].

Although Fig. 4 does not show all the available blow-off data, all the curves are characterised by a fall in δ/D_b, as U_b* increases in the subsonic regime as the gas velocity into a lifted flame increases with P_i/P_a. The fall in values becomes less severe as the choked regime is approached. This decline occurs because, as blow-off is approached, with an increasing jet velocity, the flamelets become leaner and thicker and start to extinguish, necessitating an increased pipe diameter for the overall survival of the flame. Eventually, extinctions are so extensive, that blow-off occurs at the critical diameter, D_b. As the value of δ is associated with the thickness of a premixed methane/air flame at the maximum possible burning velocity, S_L, the fall in values of δ/D_b for survival of a lifted flame is consistent with a necessary increase in D_b. These values yield the value of the minimum pipe diameter that can still sustain a lifted flame as a function of U_b*.

However, Fig. 4 shows δ/D_b attains a minimum value and then increases with U_b*. This is a characteristic of all the fuels studied over both flow regimes. The decline in δ/D_b is

always arrested in the later stages of the choked flow regime. The value ceases to fall, reaches a minimum, and then increases, in a regime that allows flames to be maintained on pipes of decreasing diameter. This suggests an increase in reactivity, after the initial decline, and is basically attributable to the complex shock structure shown in Fig. 2, and described in Section 2. It creates improved mixing at the high velocities, higher fuel mass fluxes, richer flames, and a greater reactivity arising from the shock waves.

A consequence of this is that a pipe of given diameter can experience blow-off at both a lower and a higher value of U* and P_i/P_a, for the same δ/D_b [12,13,17]. Differences in measured blow-off data amongst different workers have been attributed to the problems of measurement, sometimes under transient, rather than steady state, conditions, and also the presence of crosswinds. Birch et al. [13] were of the view that the values in [17] were underestimated, whilst those in [12] were overestimated.

3.3. Hydrogen

Normalised critical pipe diameters, δ/D_b, and P_i/P_a are presented as a function of U_b* for hydrogen jet flames, in Fig. 5. The small laminar flame thicknesses of these flames have enabled studies to be made with pipe diameters as low as 0.1 mm. Such studies are the source of experimental data for the quench regime, again drawn from [16]. Annushkin and Sverdlov [17] give experimental data over a fairly extensive range, covering subsonic and supersonic jet velocities for blow-off and flame re-attachment, as a function of the minimal pipe diameter. In this case, different fluid mechanics transformative equations are required from the Appendix, and are shown in Table 1.

Mogi and Horiguchi [18] released hydrogen at pressures of up to 40 MPa, creating jet flames on nozzles of between 0.1 and 4 mm diameter. A pilot burner ignited the hydrogen and was extinguished immediately after ignition. Blow-off conditions were measured at different pressures for burner of different diameters. After processing, these data, along with the subsonic data of Kalghatgi [15], are also plotted in the form of δ/D_b against U_b* in Fig. 5.

Again, the onset of sonic choked flow is marked by a dashed vertical line. Otherwise, the variations of δ/D_b and P_i/P_a with U_b^* are similar to those in Fig. 4. However, values of δ/D_b are about 10 times greater than those in Fig. 4, notwithstanding a low value of δ, of 0.00875 mm, compared with that for methane of 0.0413 mm. The respective values of δ_k for H_2 and CH_4 were somewhat higher, at 0.040 and 0.129 mm. This relatively greater increase for H_2 makes the associated values of δ_k/D_b even further apart.

3.4 Propane

Here the experimental data are more sparse. Annushkin and Sverdlov [17] are the principal data source, with predominantly theoretical values for P_i/P_a of up to 20. As in the case of their studies of methane, these workers give the minimal critical pipe diameters, D_b, below which blow-off occurs, and above which a lifted flame can be sustained, as a function of P_i/P_a -1. The necessary transformative equations are listed in Table 1. These theoretical values of δ/D_b are shown in Fig. 6, plotted against U_b^*. Further experimental work, in the course of the present study, provided additional data in a crucial regime. This was conducted at the State Key Laboratory of Fire Science, Hefei, described in [4], and at the Centre for Technological Risk Studies at the Polytechnic University of Catalonia, Barcelona, described in [28]. These data are also shown on this figure.

In an attempt to construct a more practical relationship, a curve parallel to the theoretical one of Annushkin and Sverdlov was constructed, based on the experimental values in [17] and also from the current study. Additional experimental subsonic data are from Kalghatgi [15]. The derived data are shown in Fig. 6, again with δ/D_b and P_i/P_a plotted against U_b^*. For the quench regime the data are again taken from [16].

Further valuable data points from jet flames at a sub-atmospheric pressure of 50 kPa are provided by the experiments of Qiang Wang et al. [29]. Figure 6 shows these data for pipe diameters of 0.8, 1, 2, 3, and 4 mm at a pressure of 50 kPa. At this pressure and 300 K, S_L=0.465 m/s [24]. The pipe diameters for Fig. 6 range between 0.1 and 10 mm.

3.5 Laminar flow, hypodermic tube, characteristics for methane, hydrogen, and propane

The regime of higher values of δ/D_b and lower values of U_b* covers microscale power generators with hypodermic tubes, the diameters of which range from 0.1 to 1.37 mm in the studies of Matta et al. [30]. At very low laminar flow values of u, a stable laminar diffusion flame can attach to the rim of the pipe. As the flow rate is increased, the increase in flame stretch rate extinguishes the diffusion flame, with localised blow-off from the burner rim, and the generation of a premixed stable lifted flame further downstream. This flame is probably very lean, with a composition close to the extinction limit, and further increase in u soon results in blow-off. With propane flames [30] this occurred when u became larger than the burning velocity of the mixture, assumed to be 0.3 m/s. A fairly small reduction in u made it impossible to sustain the lean flame, which quenched.

Figure 7 shows, for H_2, CH_4 and C_3H_8, the variations in the values of δ/D_b , above which, flame quenching occurs, and of U*, below which quenching occurs. The data for this figure were derived from the measurements of flame quenching by Cheng et al. [31] for methane, Butler et al. [16] for hydrogen, and Matta et al. [30] for propane. The references are to the data sources. Here, the plotted data were processed from the experimental data presented in [16]. As with blow-off, extinction can be avoided by an increase in pipe diameter. For comparison, the blow-off limit for CH_4 is close to U_b* = 100. These quenched flame regimes are also shown on Figs. 4 to 6 and later figures.

3.6 Comparison of CH_4, H_2, and C_3H_8 characteristics

The best fit curves to the experimental data in Figs. 4 to 6 are re-plotted together in Fig. 8. All show a similar distribution of quenched flame, lifted flame, and blow-off regimes. Although the more reactive hydrogen jet flames appear to be the most prone to quenching at low U*, they have narrower blow-off and broader lifted flame regimes. The least reactive methane has the broadest blow-off regime. At their lower values of δ/D_b with choked flow each fuel exhibits two U_b* values for a given pipe diameter, indicative of a general increase in the reactivity due to supersonic flows and shock waves.

3. 7. Subsonic jets of acetylene, butane, and ethylene

Shown in Fig. 9 are the predominantly subsonic U_b* and δ/D_b characteristics of acetylene, butane, and ethylene, derived from data in [15]. For comparative purposes, the smoothed broken curves for methane, hydrogen and propane from the previous figures in this regime are also included. The short vertical dashed lines cutting each of these curves indicate the critical pressure ratio. Again the H_2 jet exhibits the most extensive lifted flame regime, with significantly higher values of δ/D_b. The data for the hydrocarbons are closely grouped, between the methane and propane curves, with a tendency for the more reactive acetylene to have slightly higher values of δ/D_b.

4. DISCUSSION

4.1. Flame Quench and Subsonic Regimes

For many fuels flame quenching and blow-off data have been confined to the subsonic regime. Figure 9 shows that within the quench and subsonic regimes there is initially a good correlation of all the hydrocarbon blow-off data, covering ethylene, acetylene and butane, as well as the best-fit subsonic curves for H_2, CH_4 and C_3H_8, taken from Fig. 8. The quenched flame data in Fig. 7, derived for hypodermic tubes are also well correlated. In general terms, these follow the findings of the analytical and computational studies. These have shown that, in these regimes, smaller pipe diameters create better air penetration into the fuel jet, with a consequent more rapid leaning-off the fuel/air mixture. As a result, an increase in U* soon leads to extensive flame extinctions, for which the only remedial action to maintain a flame is to increase D. This effect is apparent in Fig. 9, which shows a fairly rapid decline in δ/D_b as U* increases. This decline is similar for the different hydrocarbons, but is most marked for the least reactive fuel, CH_4 and least marked for C_2H_2, C_3H_8, and, more strikingly, H_2.

As the diameter is decreased, there is a reduction in the separation between the flow numbers, U*, for flame quenching and blow-off. This is particularly so in the case of CH_4, as can be seen in Fig. 9, in which the smallest burner diameter, could be a coincidental quench and blow-off point. In the intermediate lifted flame regime between quench and blow-off, an increase in U* leads to blow-off, and a decrease leads to flame quenching.

Reynolds numbers at the pipe exit plane are less than 100 at the flame quench boundary, but approach turbulent flow magnitudes at blow-off for the larger pipe diameters. However, it is clear from Fig. 9 that hydrogen, the most reactive gas, generates a markedly narrower blow-off regime and a broader lifted flame regime, and this merited further detailed consideration.

4. 2 Hydrogen characteristics

In [27] it is suggested that the generally anomalous behaviour of hydrogen laminar flames is probably associated with the role of H atoms. These diffuse far upstream, where they can react, with the result that the preheat zone, unlike that for other gases, is not chemically inert, rendering the definition of the flame thickness more difficult [27]. This is confirmed by computed profiles of heat release rate in laminar flames plotted against the reaction progress variable. These show an almost immediate heat release in a hydrogen flame, whereas the onset of heat release occurs significantly later in a methane flame [32]. These underlying differences in the physico-chemical nature of hydrogen flames partially explain the highest values of δ_k / δ in Table 3.

Whether the use of δ_k rather than δ might improve the correlation is assessed in Fig. 10. This covers the same subsonic regime as Fig. 9, but now with the blow-off diameter below which blow-off occurs, D_b, normalised by δ_k, given by Eq. (4). The high value of δ_k / δ in Table 3 for H_2 of 4.56, creates an even greater separation of the hydrogen data from that of the other gases. However, overall, the correlation of values of δ_k / D_b for all the hydrocarbons in subsonic flow was slightly improved. No values of T^o were available for butane and, for this gas, the values for propane were employed. Reference to Fig. 8 suggests the value of D_b / δ for hydrogen is about one fifth of that for methane, at a given U*. In addition, Table 3 gives a value of δ for hydrogen that is about one fifth that for methane. This suggests that values of D_b for hydrogen at a given U* are about 25 times smaller than those for methane. Clearly, hydrogen lifted flames can be maintained down to lower values of D than hydrocarbon flames.

As a consequence of the low δ values for hydrogen jet flames, it was possible to generate perhaps the weakest flame ever measured [16], with a diameter of 0.125 mm and a power of 0.46 W, with U_b^* = 0.27 and δ/D = 0.0575. This lies on the quenched flame boundary of Figs. 5 and 7. In terms of leaks from fitted pipelines, a scarcely visible stable hydrogen flame can develop from a hydrogen pipeline leak that is as small as 0.4 μm [16]. At the other extreme, the data in Fig. 5 suggest that with U* as high as 3,000, a pipe diameter of 1 mm, and P_i/P_a = 100, the power of a hydrogen choked jet would be about 0.56 MW, with a flame height of 1 m.

4.3 Choked Flow

Outside the subsonic regime, detailed predictions are more difficult and are almost entirely dependent on experimental data. The decline in values of δ/D_b as U_b^* increases, due to increasing flamelet extinctions, is arrested by the development of choked flow, at about U_b^* = 130. This is accompanied by a marked increase in P_i/P_a, the generation of strong expansion and compression waves, as well as normal shock waves in a more reactive, combustion regime, at about U_b^* = 200.

Because of this increased reactivity, δ/D_b eventually ceases to fall, reaches a minimum, and then increases, allowing flames to be maintained on a smaller diameter pipe. This change is attributable to the high fuel mass fluxes, richer flames, improved mixing at the high velocities, and greater reactivity arising from the shock waves. A consequence of this is that blow-off with a given pipe diameter and fuel, at a given value of δ/D_b can have both low and high values of U_b^*. A flame can re-attach to the pipe [12,17] at a significantly higher P_i/P_a., at the same value of δ/D_b. The minimal value of δ/D_b yields the smallest value of D for a given fuel that can sustain lifted flames. From Fig. 8, such critical diameters are 22.9 mm for CH_4, 9 mm for C_3H_8, and 0.87 mm for H_2.

The significant structural and reactivity changes that explain the general form of the blow-off curves are not only reflected in the lift-off distances in Fig. 3, but also in the onset of the very small transition changes in flame height with increasing U* in Fig. 11, from [5]. The latter is attributed to the sharp decline in reactivity due to increasing flamelet

extinctions prior to the onset of choked flow. Resumption of increasing flame height with increasing U* is due to entry into the regime of supersonic flows.

5. CONCLUSIONS

1. There is a rapid increase in lift-off distance with U* just prior to blow-off, with the onset of flame oscillations. Where possible, the blow-off flow number, U_b*, should be the last stable value of U* prior to blow-off.

2. A new generalised mapping has been developed of jet flame regimes for flame quenching, lift-off, and blow-off, over a vast range of U* values between 0.01 and 10^4. These cover low laminar flow Reynolds numbers, increasingly turbulent flows, and shock waves.

3. These regimes are quantitatively delineated for methane, hydrogen and propane over the full range, and for acetylene, butane, and ethylene, only for unchoked flows.

4. At very low jet flows a narrow lifted flame regime exists, within which a reduction in velocity induces flame quenching, while an increase in velocity induces blow-off of weakened mixtures.

5. With increasing flow rates in the subsonic regime, the flame becomes leaner and localised extinctions develop, leading to blow-off. This can be delayed by an increase in pipe diameter. These relationships are amenable to mathematical modelling and are generalised quantitatively quite well for all the hydrocarbon fuels studied. There is a slight tendency for the more reactive mixtures to be able to support flames with slightly lower critical diameters.

6. In an attempt to reduce the differences in the correlations of the different fuels, in particular hydrogen, an improved expression was employed for the flame thickness. This brought some correlations a little closer, but not those for hydrogen.

7. There is a strikingly lower critical diameter for the blow-off of hydrogen jets, probably a consequence of the near absence of a preheat zone, due to the upstream diffusion of H

atoms. The critical diameter for blow-off with hydrogen can be about one twenty-fifth of that for methane at the same U_b*.

8. The decline in δ/D_b with increasing U_b*, is arrested in the choked flow regime due to the regions of supersonic flow and shock waves creating increased reactivity. As the jet velocity increases further, the increased reactivity enables lifted flames to be sustained at smaller diameters.

9. As a consequence, for a given pipe, there can be blow-off at a lower value of U_b* and re-attachment at a higher value.

APPENDIX: Jet Fluid Mechanics

i indicates upstream stagnation conditions.

Acoustic velocity, a, = $(P\gamma/\rho)^{0.5} = (\gamma RT)^{0.5}$, (1A)

with R the mass specific gas constant equal to the Universal Gas Constant of 8.314 J/mol· K divided by the molecular weight of the gas, and γ the ratio of specific heats.

In choked flow, for a perfect gas with sonic velocity, a, the Critical Pressure Ratio, CPR,

$P/P_i = (2/(\gamma+1))^{(\gamma/(\gamma-1))}$. (2A)

Now, the Mach number, M = u/a (3A)

and, $T/T_i = (P/P_i)^{(\gamma-1)/\gamma}$. (4A)

From Eq. (1A)

$(a/a_i)^2 = (\gamma T/\gamma_i T_i) = (P/P_i)^{(\gamma-1)/\gamma}$, with $\gamma = \gamma_i$. (5A)

From Eqs. (3A) and (5A)

$u^2 = M^2a^2 = M^2a_i^2(P/P_i)^{(\gamma-1)/\gamma}$, and (6A)

$P_i/P = (Ma_i/u)^{2\gamma/(\gamma-1)}$. (7A)

Euler's equation for isentropic flow gives [33]

$$\left(\gamma/\left(\gamma-1\right)\right)P/\rho + u^2/2 = \left(\gamma/\left(\gamma-1\right)\right)P_i/\rho_i . \quad (8A)$$

From Eqs. (3A), (8A) and (1A)

$$M^2a^2/2 = \left(\gamma/\left(\gamma-1\right)\right)\left(P_i/\rho_i - P/\rho\right) = \left(1/\left(\gamma-1\right)\right)\left(a^2{}_i - a^2\right). \quad (9A)$$

$$M^2 = \left(2/\left(\gamma-1\right)\right)\left(a_i^2/a^2 - 1\right). \quad (10A)$$

Hence from Eqs. (5A) and (10A)

$$M^2 = (2/(\gamma-1))\left((P_i/P)^{(\gamma-1)/\gamma} - 1\right) \text{ and} \quad (11A)$$

$$\frac{P_i}{P_a} = \left[\frac{M^2\left(\gamma-1\right)+2}{2}\right]^{\left(\gamma/\gamma-1\right)}. \quad (12A)$$

From Eqs. (11A) and (6A)

$$u^2 = M^2a_i^2\left(M^2\left(\gamma-1\right)+2\right)/2\Big)^{-1}, \quad (13A)$$

$$\left(\gamma-1\right)+2/M^2 = 2a_i^2/u^2, \quad (14A)$$

and

$$M = (a_i^2/u^2 - (\gamma-1)/2)^{-0.5}. \quad (15A)$$

When choked flow occurs, the value of M at the pipe exit is unity and u is given by a in Eq. (1A), with T at ambient temperature.

ACKNOWLEDGEMENTS

A.P. gratefully acknowledges the financial support of the Royal Society in the form of a Postdoctoral Newton International Fellowship. Professor Joaquim Casal at the Centre for Technological Risk Studies at the Polytechnic University of Catalonia at Barcelona, and Professor Longhua Hu at the State Key Laboratory of Fire Science, Hefei, are thanked for

the use of their experimental facilities, to obtain propane and methane blow-off data, respectively.

REFERENCES

1. Qiang. Wang, Longhua. Hu, Sung. Hwan. Yoon, Shouxiang. Lu, M. Delichatsios, Suk. Ho. Chung, Blow-out limits of nonpremixed turbulent flames in a cross flow at atmospheric and sub-atmospheric pressures, Combust. Flame 162 (2015) 3562-3568.
2. M.R. Johnson, L.W. Kostiuk, A parametric model for the efficiency of a flame in crosswind, Proc. Combust. Inst. 29 (2002) 1943-1950.
3. Z. Chen, S. Ruan, N. Swaminathan, Simulation of turbulent lifted methane jet flames: effects of air dilution and transient flame propagation, Combust. Flame 162 (2015) 703-716.
4. A. Palacios, D. Bradley, L Hu, Lift-off and blow-off of methane and propane subsonic vertical jet flames, with and without diluent air, 183 Fuel (2016) 414-419.
5. D. Bradley, P.H. Gaskell, X.J. Gu, A. Palacios, Jet flame heights, lift-off distances, and mean flame surface density for extensive ranges of fuels and flow rates, Combust. Flame 164 (2016) 400-409.
6. K.M Lyons, Towards an understanding of the stabilization mechanisms of lifted turbulent jet flame experiments, Prog. Energy Combust. Sci. 33 (2007) 211-231.
7. N. Peters, Turbulent Combustion, University Press, Cambridge, 2000.
8. D. Bradley, P.H. Gaskell, X.J. Gu, The mathematical modeling of lift-off and blowoff of turbulent non-premixed methane jet flames at high strain rates, Proc. Combust. Inst. 27 (1998) 1199-1206.
9. D. Bradley, M. Lawes, Kexin Liu, M.S. Mansour, Measurements and correlations of turbulent burning velocities over wide ranges of fuels and elevated pressures, Proc. Combust. Inst. 34 (2013) 1519-1526.
10. D. Bradley, D.R. Emerson, P.H. Gaskell, X.J Gu, Mathematical modelling of turbulent non-premixed piloted-jet flames with local extinctions, Proc. Combust. Inst. 29 (2002) 2155-2162.
11. B.C. Ewan, K. Moodie, Structure and velocity measurements in underexpanded jets, Combust. Sci. Tech. 45 (1986) 275-288.
12. B.J. McCaffrey, D.D. Evans, Very large methane jet diffusion flames, Proc. Combust. Inst. 21 (1986) 25-31.
13. A.D. Birch, D.R. Brown, D.K. Cook, G.K. Hargrave, Flame stability in underexpanded natural gas jets, Combust. Sci. Tech 58 (1988) 267-280.
14. A.D. Birch, J. Hughes, F. Swaffield, Velocity decay of high pressure jets, Combust. Sci. and Tech. 52 (1987) 161-171.
15. G.T. Kalghatgi, Blow-out stability of gaseous jet diffusion flames Part I: In still air, Combust. Sci. Tech. 26 (1981) 233-239.
16. M.S. Butler, C.W. Moran, P.B. Sunderland, R.L. Axelbaum, Limits for hydrogen leaks that can support stable flames, Int. Jour. of Hydrogen Energy 34 (2009) 5174-5182.
17. Y.M. Annushkin, E.D. Sverdlov, Stability of submerged diffusion flames in subsonic and underexpanded supersonic gas-fuel streams, Combust. Explos. Shock Waves 14(5) (1978) 597-605.

18. T. Mogi, S. Horiguchi, Experimental study on the hazards of high-pressure hydrogen jet diffusion flames, J. Loss Prevent. Proc. 22 (2009) 45-51.
19. C.J. Sun, C.J. Sung, L. He, C.K. Law, Dynamics of weakly stretched flames: quantitative description and extraction of global flame parameters, Combust. Flame 118 (1999) 108-128.
20. X.J. Gu, M.Z. Haq, M. Lawes, R Wooley, Laminar burning velocity and Markstein lengths of methane-air mixtures, Combust. Flame 121 (2000) 41-58.
21. F.N. Egolfopoulos, D.L. Zhu, C.K. Law, Experimental and numerical determination of laminar flame speeds: mixtures of C2-hydrocarbons with oxygen and nitrogen, Proc. Combust. Inst. 23 (1990) 471-478.
22. K. Kumar, G. Mittal, C.J. Sung, C.K. Law, An experimental investigation of ethylene/O2/diluents mixtures: laminar flame speeds with preheat and ignition delays at high pressures, Combust. Flame 153 (2008) 343-354.
23. K.J. Bosschaart, L.P.H. De Goey, The laminar burning velocity of flames propagating in mixtures of hydrocarbons and air measured with the heat flux method, Combust. Flame 136 (2004) 261-269.
24. D. Razus, D. Oancea, V. Brinzea, M. Mitu, C. Movileanu, Experimental and computed burning velocities of propane-air mixtures, Energy Convers. Manage. 51(12) (2010) 2979-2984.
25. S.G. Davis, C.K. Law, Determination of and fuel structure effects on laminar flame speeds of C1 to C8 hydrocarbons, Combust. Sci. and Tech. 140 (1998) 427-449.
26. C. Morley GasEq: a chemical equilibrium program for windows; 2005. <http:// www.gaseq.co.uk>.
27. J. Göttgens, F. Mauss, N. Peters, Analytic approximations of burning velocities and flame thicknesses of lean hydrogen, methane, ethylene, ethane, acetylene and propane flames, Proc. Combust. Inst. 24 (1992) 129-135.
28. A. Palacios, M. Muñoz, J. Casal, Jet fires: an experimental study of the main geometrical features of the flame in subsonic and sonic regimes, AIChE J. 55(1) (2009) 256-263.
29. Qiang. Wang, Longhua. Hu, Suk. Ho. Chung, Blow-out of nonpremixed turbulent jet flames at sub-atmospheric pressures, Combust. Flame 176 (2017) 358-360.
30. L.M. Matta, Y. Neumeier, B. Lemon, B.T Zinn, Characteristics of microscale diffusion flames, Proc. Combust. Inst. 29 (2002) 933-939.
31. T.S. Cheng, C.P. Chen, C.S. Chen, Y.H. Li, C.Y. Wu, Y.C Chao, Characteristics of microjet methane diffusion flames, Combust. Theory and Modeling, 10(6) (2006) 861-881.
32. D. Bradley, S.E-D. Habik, S.A. El-Sherif, A generalisation of laminar burning velocities and volumetric heat release rates, Combust. Flame 87 (1991) 336-345.
33. B.S. Massey, Mechanics of Fluids, Sixth edition, 1989, Van Nostrand Reinhold (International).

TABLE AND FIGURE CAPTIONS
Tables

Table 1. Transformative Flow Equations employed in deriving Dimensionless Groups.
Table 2. Physicochemical Constants. All values at 300 K, 0.1 MPa, except for $C_3H_8{}^*$, which is for 300 K and 50 kPa.
Table 3. Laminar Preheat Zone Thicknesses at S_L, at 0.1 MPa, except for $C_3H_8{}^*$ which is at 50 kPa.

Figures

(a) Normalised mean lift-off distances, (L/D)f, as blow-off is approached, as a function of U*.

(b) Oscillations of L, leading up to blow-off. Time interval between successive data points is 0.25 s. From [4].

Figure 1. Methane jet flames showing: (a) Increasing lift-off distance, as blow-off is approached with increasing U*, and (b) lift-off distance oscillations, prior to blow-off.

Figure 2. Principal regions around the nozzle exit (for an underexpanded jet). Reproduced from [11].
Figure 3. Normalised flame lift-off distances for the separated subsonic (left ordinate) and choked/supersonic (right ordinate) regimes. Modified from [5].
Figure 4. Methane Jet Flame Blow-off Boundaries. Increasing δ/D above δ/D_b leads to blow-off. Dashed vertical line shows Critical Pressure Ratio conditions.
Figure 5. Hydrogen Jet Flame Blow-off Boundaries. Increasing δ/D above δ/D_b leads to blow-off. Dashed vertical line shows Critical Pressure Ratio conditions.
Figure 6. Propane Jet Flame Blow-off Boundaries. Increasing δ/D above δ/D_b leads to blow-off. Dashed vertical line shows Critical Pressure Ratio conditions.
Figure 7. Regime of flame quenching for, hydrogen, methane and propane.
Figure 8. Methane, Hydrogen and Propane Jet Flame Blow-off and Quench Boundaries. Increasing δ/D above δ/D_b leads to blow-off or quench. Dashed vertical lines show Critical Pressure Ratio conditions.
Figure 9. Sonic and subsonic Jet Flame Blow-off and Quench Boundaries, based on δ/D_b, for methane, hydrogen and propane. Subsonic blow-off boundaries are shown for acetylene, butane and ethylene. Increasing δ/D above δ/D_b leads to blow-off or quench. Dashed vertical lines show Critical Pressure Ratio conditions.
Figure 10. Sonic and subsonic Jet Flame Blow-off and Quench Boundaries, based on δ_k/D_b, for methane, hydrogen and propane. Subsonic blow-off boundaries are shown

for acetylene, butane and ethylene. Increasing δ_k/D above δ_k/D_b leads to blow-off or quench. Dashed vertical lines show Critical Pressure Ratio conditions.
Figure 11. Normalised flame height, H/D, showing the transition region, with little change in height, as a function of U*. From [5].

Table 1. Transformative Flow Equations employed in deriving Dimensionless Groups.

Data Source	Appendix Equation Numbers	
McCaffrey and Evans [12]	14A	11A
Birch et al. [13,14]	6A	9A
Kalghatgi [15]	9A	12A
Butler et al. [16]	3A	12A
Annushkin and Sverdlov [17]	14A	11A
Mogi and Horiguchi [18]	9A	12A

Table 2. Physicochemical Constants. All values at 300 K, 0.1 MPa, except for $C_3H_8{}^*$, which is for 300 K and 50 kPa.

Gas	γ 300K, 0.1MPa	ν (m^2/s) at 300K, 0.1MPa	S_L (m/s)
H_2	1.4	$2.56 \cdot 10^{-5}$	3.03 [19]
CH_4	1.3	$1.61 \cdot 10^{-5}$	0.39 [20]
C_2H_2	1.23	$0.96 \cdot 10^{-5}$	1.57 [21]
C_2H_4	1.24	$2.11 \cdot 10^{-5}$	0.72 [22]
C_3H_8 $C_3H_8{}^*$	1.365 1.365^*	$1.47 \cdot 10^{-5}$ $2.95\ 10^{-5*}$	0.43 [23] 0.465^*[24]
C_4H_{10}	1.1	$3.77 \cdot 10^{-5}$	0.41 [25]

Table 3. Laminar Preheat Zone Thicknesses at S_L, at 0.1 MPa, except for $C_3H_8{}^*$ which is at 50 kPa.

Fuel	ϕ	S_L (m/s)	T^o [27] K	δ mm	δ_k mm	δ_k/δ
H_2	1.8	3.03	1000	0.0087459	0.03985	4.56
CH_4	1.02	0.39	1220	0.041282	0.1288	3.12
C_3H_8	1.1	0.43	1180	0.034186	0.100452	2.94
$C_3H_8{}^*$	1.1^*	0.465^*	1160^*	0.0634^*	0.1842^*	2.91^*
C_2H_2	1.4	1.57	1040	0.009618	0.027542	2.86
C_2H_4	1.1	0.72	1120	0.021111	0.062198	2.95

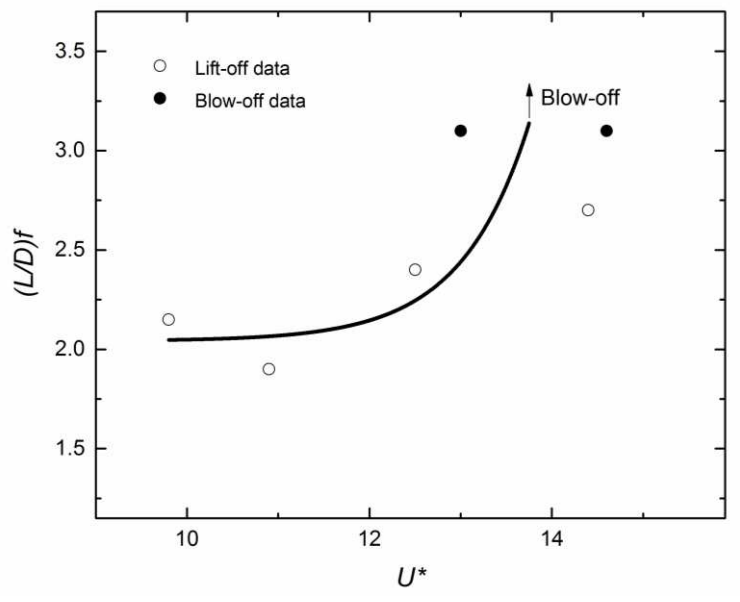

(a) Normalised mean lift-off distances, (L/D)f, as blow-off is approached, as a function of U*.

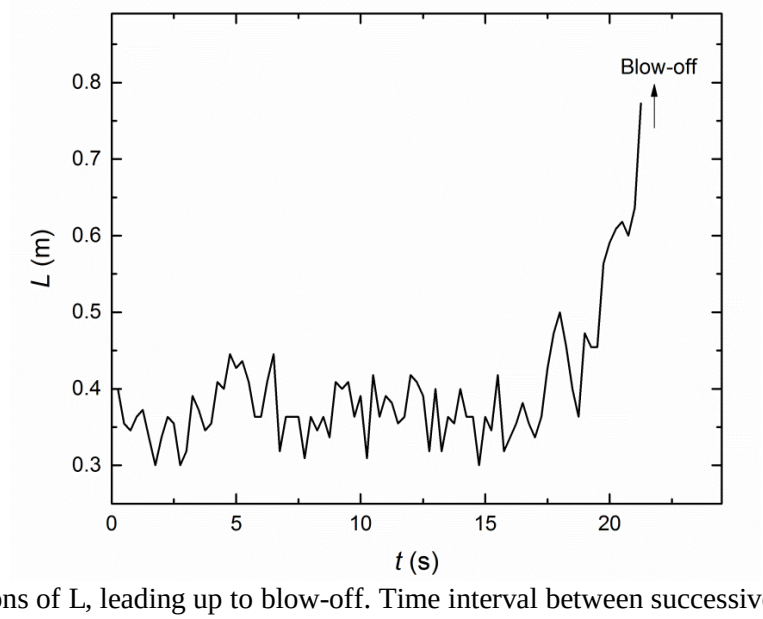

(b) Oscillations of L, leading up to blow-off. Time interval between successive data points is 0.25 s. From [4].

Figure 1. Methane jet flames showing: (a) Increasing lift-off distance, as blow-off is approached with increasing U*, and (b) lift-off distance oscillations, prior to blow-off.

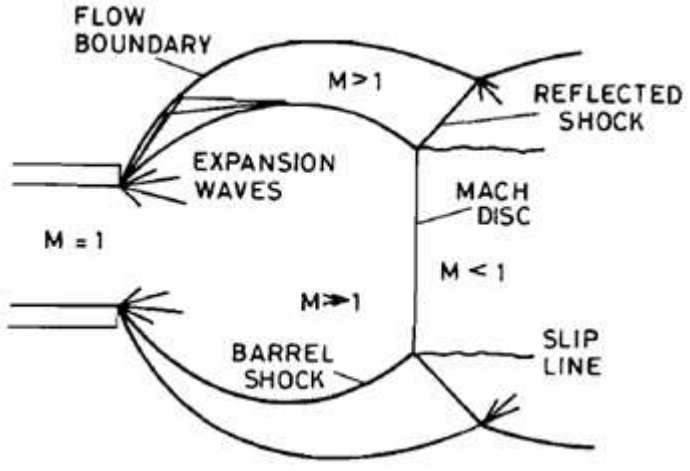

Figure 2. Principal regions around the nozzle exit (for an underexpanded jet). Reproduced from [11].

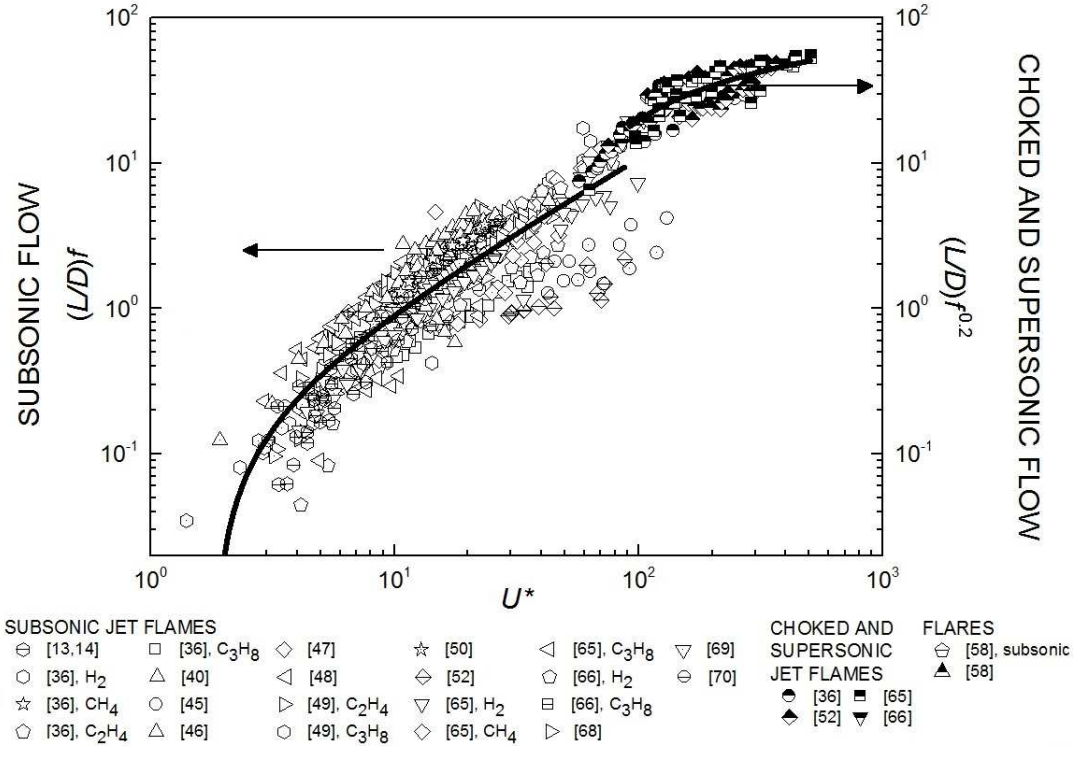

Figure 3. Normalised flame lift-off distances for the separated subsonic (left ordinate) and choked/supersonic (right ordinate) regimes. Modified from [5].

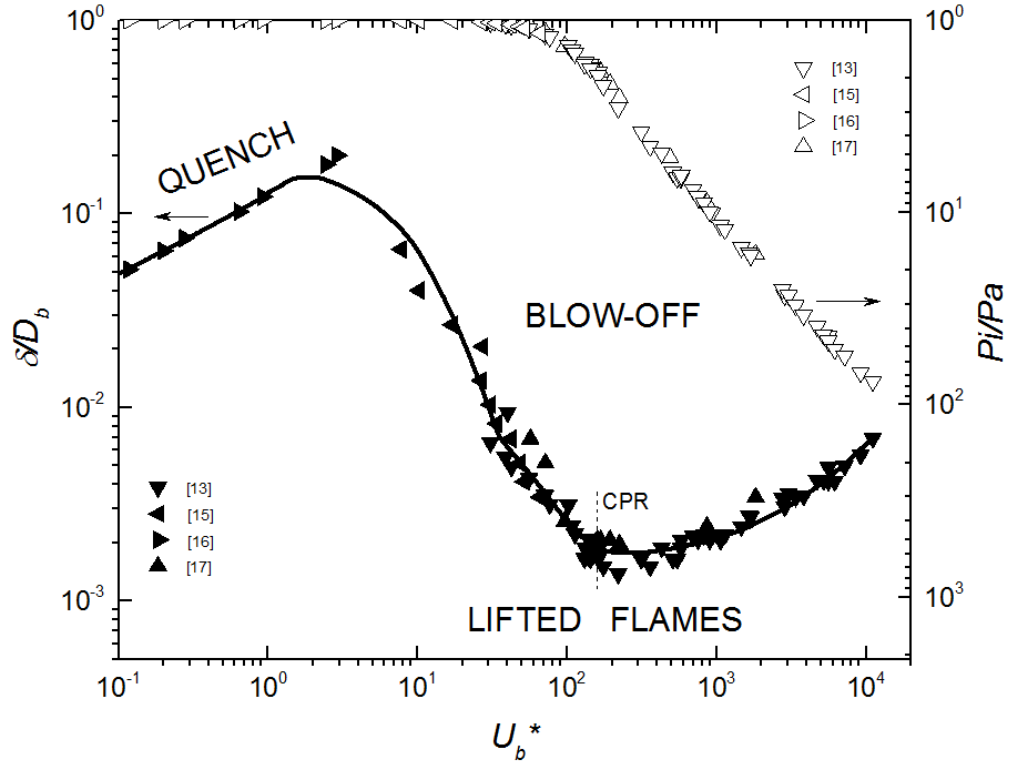

Figure 4. Methane Jet Flame Blow-off Boundaries. Increasing δ/D above $\delta/\mathrm{D_b}$ leads to blow-off. Dashed vertical line shows Critical Pressure Ratio conditions.

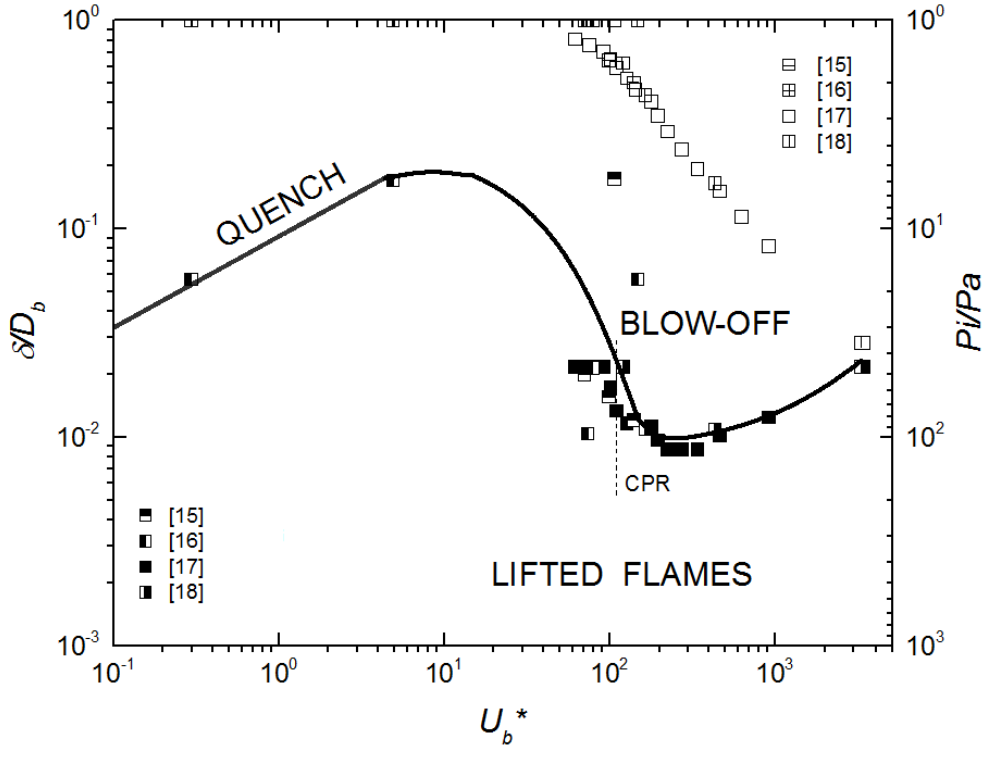

Figure 5. Hydrogen Jet Flame Blow-off Boundaries. Increasing δ/D above $\delta/\mathrm{D_b}$ leads to blow-off. Dashed vertical line shows Critical Pressure Ratio conditions.

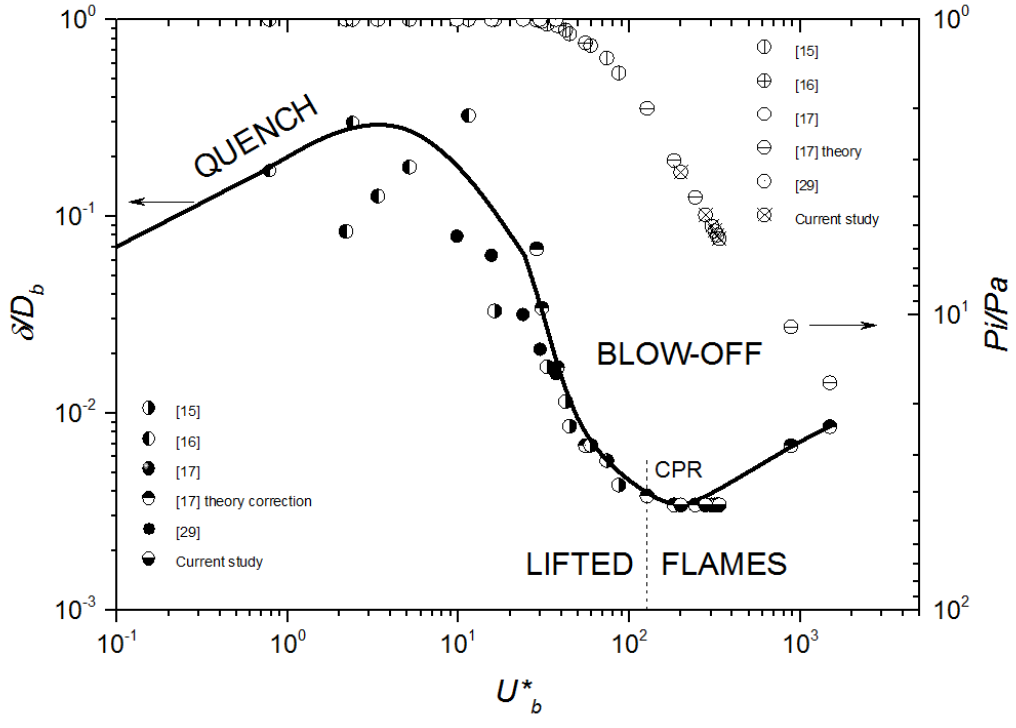

Figure 6. Propane Jet Flame Blow-off Boundaries. Increasing δ/D above $\delta/\mathrm{D_b}$ leads to blow-off. Dashed vertical line shows Critical Pressure Ratio conditions.

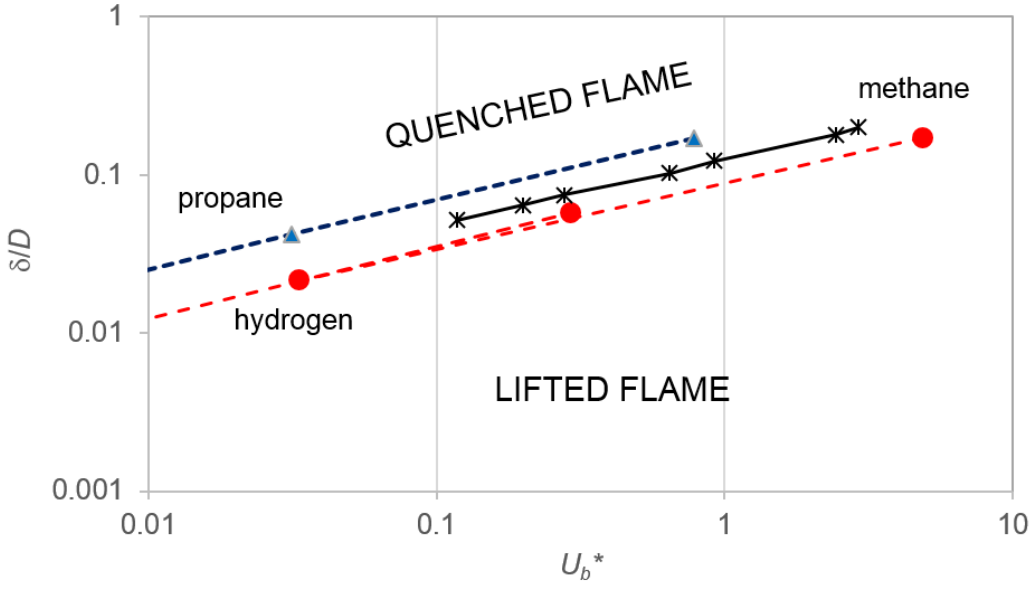

Figure 7. Regime of flame quenching for, hydrogen, methane and propane.

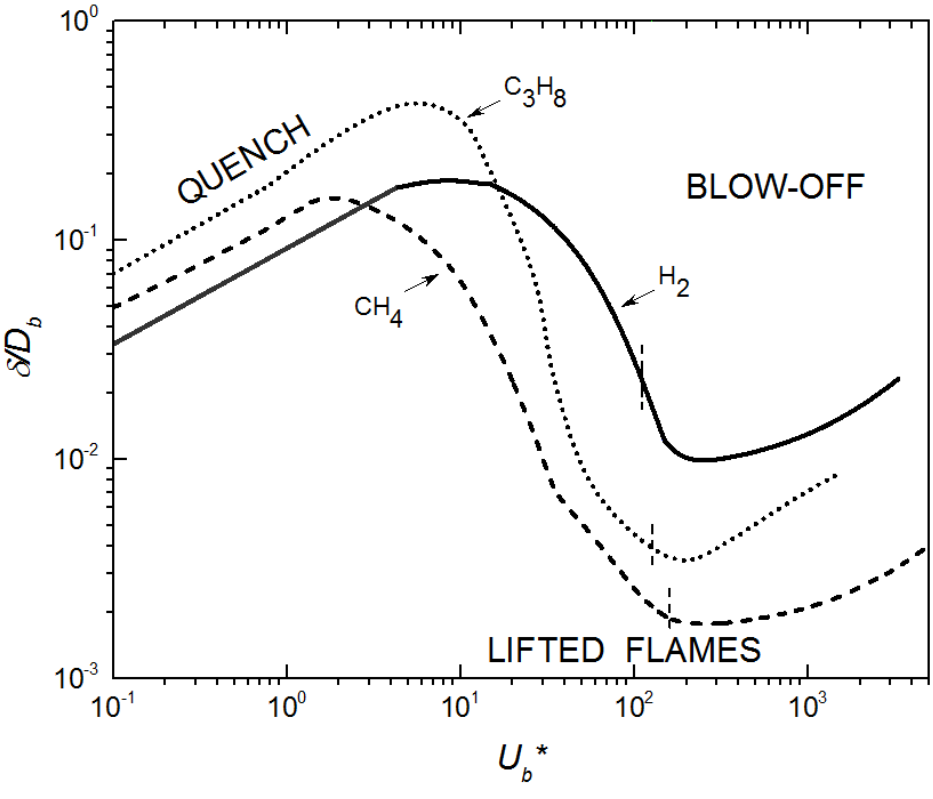

Figure 8. Methane, Hydrogen and Propane Jet Flame Blow-off and Quench Boundaries. Increasing δ/D above $\delta/\mathrm{D_b}$ leads to blow-off or quench. Dashed vertical lines show Critical Pressure Ratio conditions.

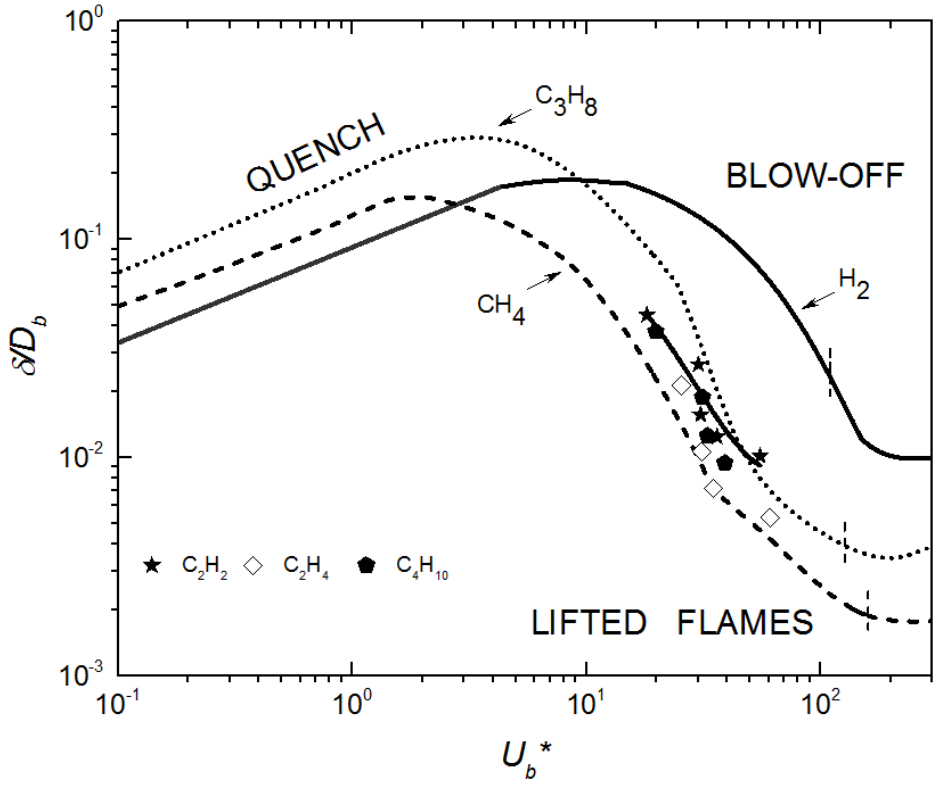

Figure 9. Sonic and subsonic Jet Flame Blow-off and Quench Boundaries, based on $\delta/\mathrm{D_b}$, for methane, hydrogen and propane. Subsonic blow-off boundaries are shown for acetylene, butane and ethylene. Increasing δ/D above $\delta/\mathrm{D_b}$ leads to blow-off or quench. Dashed vertical lines show Critical Pressure Ratio conditions.

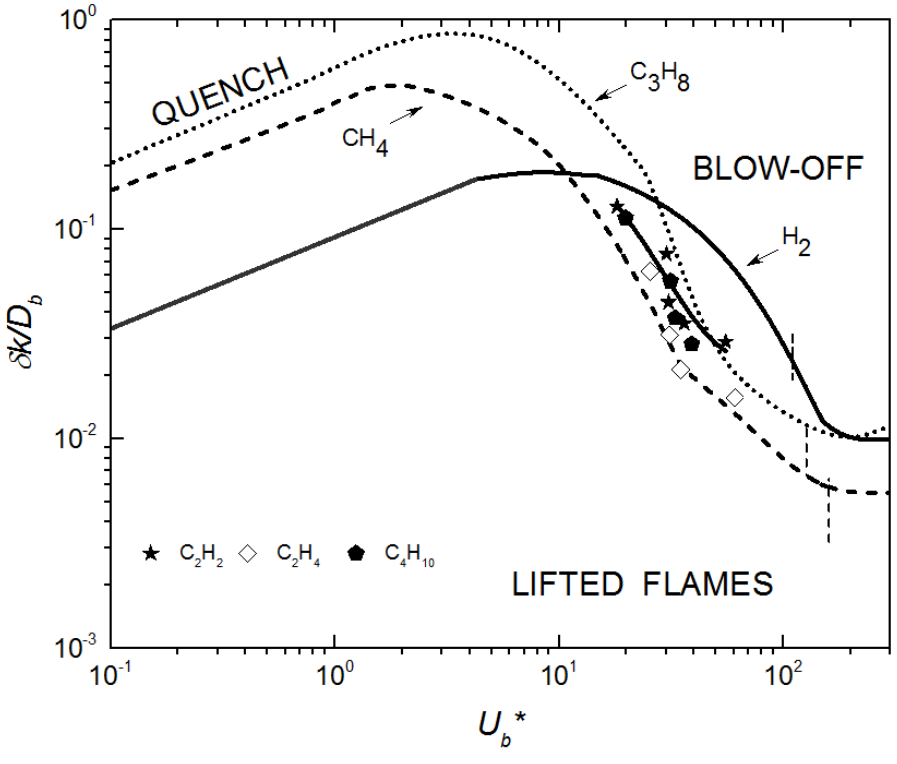

Figure 10. Sonic and subsonic Jet Flame Blow-off and Quench Boundaries, based on δ_k / D_b, for methane, hydrogen and propane. Subsonic blow-off boundaries are shown for acetylene, butane and ethylene. Increasing δ_k/D above δ_k / D_b leads to blow-off or quench. Dashed vertical lines show Critical Pressure Ratio conditions.

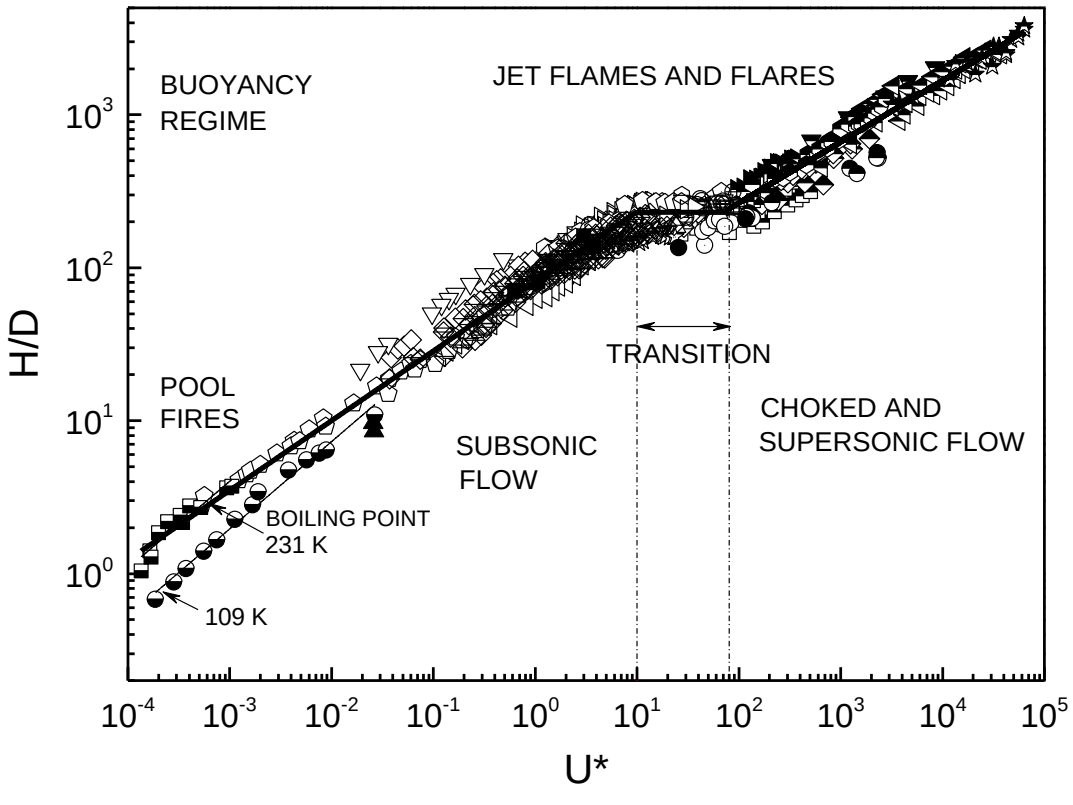

Figure 11. Normalised flame height, H/D, showing the transition region, with little change in height, as a function of U*. From [5].